NATURE OF ANTIPROTON PRODUCTION IN HIGH ENERGY NUCLEAR COLLISIONS: ASSORTED DATA VERSUS SPECIFIC MODELS

P. GUPTAROY* and D. P. BHATTACHARYYA†

Department of Theoretical Physics,
Indian Association for the Cultivation of Science, Kolkata 700032, India
†*tpdpb@mahendra.iacs.res.in*

BHASKAR DE and S. BHATTACHARYYA‡

Physics and Applied Mathematics Unit (PAMU),
Indian Statistical Institute, Kolkata 700035, India
‡*bsubrata@www.isical.ac.in*

Received 8 November 2001

We attempt here to deal with some of the important characteristics of secondary antiproton production in various high energy nuclear interactions on the basis of a model for production of particles in PP collisions. The results have, thereafter, been converted to those for AA collisions through an appropriate mechanism. The effect of rescattering and cascading in the production processes and on the chosen models has also been incorporated in a phenomenological manner. Comparison of the calculated results with data on the relevant observables leads to a striking agreement and this fair success is claimed here to obviously signal the strength of the basic models that are applied in the present work.

Keywords: Relativistic heavy ion collisions; inclusive production; quark gluon plasma.

PACS numbers: 25.75.-q, 13.85.Ni, 12.38.Mh

1. Introduction

Antiproton ($\bar{p}$) yield in relativistic heavy ion collisions is supposed to be determined by two consecutive processes, viz., initial production in nucleon–nucleon collisions and subsequent annihilation of them in their collisions with the surrounding nucleons.[1] The relevant observable, in this context, is the number of participating nucleons in the nucleus which cause the production of the particles including secondary antiprotons. Against this background, an anomalously large $\bar{p}$ yield has been predicted as one of the most important diagnostics for the experimental

*On leave from Department of Physics, Raghunathpur College, PO Raghunathpur 723133, Dist.: Purulia (WB), India.

detection of Quark Gluon Plasma (QGP).[2] The $\bar{p}$ production, in the framework of the QGP hypothesis, has also been suggested as a signal and measure of high baryon density.[3] However, despite the very recent claims[4] on some indirect evidence for the formation of a quark gluon plasma at higher energies, unambiguous signals of a phase transition into an equlibrated QGP state are still missing.[5] Thus, by measuring antiproton production systematically, it may be possible, one assumes, to disentangle the effects of production, absorption and the problem of baryon number transport[6–9] of both baryons and antibaryons. All these expectations and predictions gradually lead to the successive measurements of the $\bar{p}/p$ ratios within the precincts of laboratory-based heavy ion experiments. Thus, this ratio factor, $\bar{p}/p$, in the process, assumes both special significance and paramount importance.

In the recent past, different groups, like E802 collaboration at AGS,[1] NA49 collaboration in SPS,[10] Adler *et al.*, STAR, and PHENIX collaborations etc. at RHIC[9,11,12] reported measurements of various observables for different high energy heavy ion collisions. We will concentrate here on some of the important observables involving production of real secondary antiprotons in nucleus–nucleus collisions.

Our objective, here, is to interpret a part of data obtained in the latest heavy ion experiments[1,8–12] from the viewpoint of a model with no direct QGP tag and on the basis of some ancillary physical ideas incorporated therein. We would also like to examine the capability of the chosen model to deal with the very up-to-date data on particle production in high energy heavy nucleus–nucleus collisions. Thus, the study could serve twin purposes: (i) explaining the new data-sets on antiproton production; (ii) throwing a well-focused light on the degree of validity of the approach or approaches resorted to for the present work.

The plan of the paper is as follows. In Subsec. 2.1 we present the synopsis of the model that we would like to apply here for the present study. Subsection 2.2 deals with the issues on the link-up between PP and AA reactions. In Sec. 3 we focus on the results obtained and their model-based interpretations. Section 4 encompasses the summary of final conclusions to be drawn from the present model-based study.

2. Nucleon–Nucleon Collisions and Nucleus–Nucleus Interactions: The Approach

In this section, at first, we deal with the production of particles in nucleon–nucleon (NN) interactions. Thereafter, we put forward the approach to convert the results of NN collisions to the values for the case(s) nucleus–nucleus collisions.

2.1. *The specific multiple production model in PP collisions: A brief sketch*

We will use here a particular version of Sequential Chain Model (SCM)[13–15] to study some of the main characteristics and observations related to production of pi-mesons and antiprotons in different collisions at high energies. Let us first recapitulate some of the salient features and important physical characteristics of

the SCM valid for hadron–hadron and lepton–hadron collisions. According to this model, high energy hadronic interactions boil down, essentially, to the pion–pion interactions; as the protons are conceived in this model as $P = (\pi^+\pi^0 C)$, where C is a spectator particle needed for the dynamical generation of quantum numbers of the nucleons. The production of pions in the present scheme occurs as follows. The incident energetic pi-mesons in the structure of the projectile proton (nucleon) emits a rho meson in the interacting field of the pion lying in the structure of the target proton, the rho meson then emits a pi-meson and is changed into an omega meson, the omega meson then again emits a pi-meson and is transformed once again into a rho-meson and thus the process of production of pion-secondaries continue in the sequential chain of rho-omega-pi mesons. The production of baryon–antibaryon pairs takes place through the decay of secondary pi-mesons. The kaon secondaries are produced by decays of phi-zero mesons which are generated in a manner similar to the production of pions with a rho-pi-phi-zero chain. There are specific mechanisms for production of the various other secondary particles as well in high energy hadronic/nuclear collisions. Obviously, all the calculations to be made with the help of this model are based on the applications of the concepts of the Quantum Field Theory (QFT) and the Feynman diagram techniques. For the present paper we would simply pick up the relevant results from some of our previous work[13–15] wherein the details of calculations would be available for any interested reader.

The major achievements of this model (SCM) are:

(i) It gives a nearly dynamical description of the processes for production of particles in high energy NN collisions, as the model (SCM) under consideration here contains a single hand-inserted parameter; and this parameter involves the relationship between sum of the square of the momenta of the specific variety of the secondaries, the pion-mass and c.m. energy.

(ii) The model presents a unified picture of both low and large transverse momentum phenomenon and admits no compartmentalization between "soft" and "hard" production of particles which are some artifacts imposed by the constraints of QCD-physics.

(iii) It envisages the "jet" structure for the particle production mechanisms as the two-sided ⟨⟨sprays⟩⟩ of the secondary hadrons.

(iv) The model caters successfully to the data on the cardinal multiparticle observables like average multiplicity, average transverse momenta of the produced particles and on the inclusive production of the secondaries in terms of both $x(y)$ or p_T-variable.

(v) The model introduces the violation of the Feynman scaling in an in-built manner with a generalized form of the power laws of multiplicities for the various secondaries.

(vi) The model nicely explains the extremely slow rise of the K/π ratio with c.m. energy.

(vii) It explains successfully the by-now established "leading particle effect (LPE)" and the "inelasticity" behavior in high energy particle production.
(viii) The model does also accommodate the features of the "Seagull effect" in a somewhat limited manner.
(ix) The particle ratios and the ratios of inclusive cross-sections are also modestly well-reproduced by this model.
(x) The model subscribes to the property of ⟨⟨universality⟩⟩ of all high energy interactions in a very straightforward and clear-cut manner.

Now let us proceed to present a summary of some of the useful results to be utilized here for the present work. It is to be noted that the assorted expressions given below are derived here on of rigorous field-theoretic considerations for the inclusive production cross-sections and average multiplicity values of the various types of secondary pions (of any variety) and of antiprotons produced in the sequential chain in the above-stated manner. The obtained formulae are being given by the following sets of relations[13–15] wherein p_T and x are the transverse momentum and the Feynman scaling variable respectively, and $\sqrt{s}$ is the c.m. energy for PP-system. Besides, by definition, $x = 2p_L/\sqrt{s}$ where p_L is the longitudinal momentum of the particle.

For any variety of secondary pions (π^+, π^- or π^0) we have

$$E\frac{d^3\sigma}{dp^3}\bigg|_{PP\to\pi^- x} \cong C_{\pi^-}\exp\left(\frac{-26.88p_T^2}{\langle n_{\pi^-}\rangle_{PP}(1-x)}\right)\exp(-2.38\langle n_{\pi^-}\rangle_{PP}x)\,, \tag{1}$$

where $|C_\pi| \cong 90$ for ISR energy region, but for $P\bar{P}$ collider energy it increases with the increase of inelastic cross-section and it is different for different energy region and where

$$\langle n_{\pi^+}\rangle_{PP} \cong \langle n_{\pi^-}\rangle_{PP} \cong \langle n_{\pi^0}\rangle_{PP} \cong 1.1s^{1/5}\,, \tag{2}$$

for very high energies, and at low p_T

$$E\frac{d^3\sigma}{dp^3}\bigg|_{PP\to\pi^- x} \cong E\frac{d^3\sigma}{dp^3}\bigg|_{PP\to\pi^+ x} \cong E\frac{d^3\sigma}{dp^3}\bigg|_{PP\to\pi^0 x}\,. \tag{3}$$

For, low-p_T antiproton production in PP scattering at high energies the derived expression for inclusive cross-section is

$$E\frac{d^3\sigma}{dp^3}\bigg|_{PP\to\bar{p}x} \cong C_{\bar{p}}\exp\left(\frac{-0.66[(p_T^2)_{\bar{p}}+m_{\bar{p}}^2]}{\langle n_{\bar{p}}\rangle_{PP}^{3/2}(1-x)}\right)\exp(-25.4\langle n_{\bar{p}}\rangle_{PP}x)\,, \tag{4}$$

with $|C_{\bar{p}}| \cong 1.87\times10^3$ and for ultrahigh energies

$$\langle n_{\bar{p}}\rangle_{PP} \cong \langle n_p\rangle_{PP} \cong 2\times10^{-2}s^{1/4}\,, \tag{5}$$

and at low-p_T

$$E\frac{d^3\sigma}{dp^3}\bigg|^{nls}_{PP\to\bar{p}x} \cong E\frac{d^3\sigma}{dp^3}\bigg|^{nls}_{PP\to px}\,. \tag{6}$$

Here, nls stands for *nonleading-secondaries*.

Now, for the calculation of rapidity distribution from these set of equations for different observables we can make use of two standard formulae from Ref. 16. The first relation is from $Ed^3\sigma/dp^3$ to $d\sigma/dy$,

$$\left.\frac{d\sigma}{dy}\right|_{PP} = \left[\int E\left.\frac{d^3\sigma}{dp^3}\right|_{PP} d^2p_T\right], \tag{7}$$

and the second one is from $d\sigma/dy$ to dN/dy, viz.,

$$\left.\frac{dN}{dy}\right|_{PP} = \frac{1}{\sigma_{\text{inel}}}\left.\frac{d\sigma}{dy}\right|_{PP}. \tag{8}$$

The letters and symbols have their standard contextual connotation. And for any inclusive reaction, the relationship between x, the Feynman scaling variable and y, the rapidity variable, is given by the undernoted form[17]

$$x \simeq \frac{2p_{z\text{cm}}}{\sqrt{s}} = \frac{2m_T \sinh y_{\text{cm}}}{\sqrt{s}}. \tag{9}$$

By applying Eqs. (7)–(9) into Eqs. (1) and (4) we get the rapidity distributions dN/dy for the secondary particles like pions and antiprotons for nucleon–nucleon interactions at ultra-high energies.

2.2. *Nucleus–nucleus collisions and nucleon–nucleon interactions: The fly-over at high energies*

In order to build the bridge between nucleon–nucleon interactions and the nucleus–nucleus collisions, we proceed in the method suggested by Wong.[18] As a first step in the process we will have to consider a nuclear reaction $A+B \to C+X$, where A and B are projectile and target nucleus respectively. In a reaction of this type, for the impact parameter b, we assume, there are $n'(b)$ number of inelastic nucleon–nucleon collisions. Each collision contributes to the production of particles. On the basis of the assumption that all the collisions contribute in the same way, the rapidity distribution dN/dy for the nucleus–nucleus collisions would have a relationship with the rapidity distribution dN/dy for the nucleon–nucleon collisions; and that is expressed in the following form:

$$\left.\frac{dN(b)}{dy}\right|_{AB} \cong \frac{n'(b)}{1+a(A^{1/3}+B^{1/3})}\left.\frac{dN}{dy}\right|_{PP}, \tag{10}$$

where a is a parameter that is to be chosen. For example, a is taken here ~ 0.09.

The expression for $n'(b)$ is given by

$$n'(b) = \frac{ABT(b)\sigma_{in}}{(1-[1-T(b)\sigma_{in}]^{AB})} \tag{11}$$

with $T(b)$, the thickness function, that can be estimated by a Gaussian distribution

$$T(b) = \frac{1}{2\pi\beta^2} e^{-b^2/2\beta^2}, \tag{12}$$

where

$$\beta^2 = \beta_A^2 + \beta_B^2 + \beta_p^2, \tag{13}$$

and

$$\beta_A = \frac{r_0' A^{1/3}}{\sqrt{3}} \tag{14}$$

with $r_0' = 1.05$ fm, and β_p, the thickness function parameter for nucleon–nucleon collision, is 0.68 fm. For central collisions, $T(b)$ does not vanish and the denominator can be approximated to unity. Furthermore, one can neglect β_p which is small in comparison with β_A and β_B. Therefore, we get

$$\left.\frac{dN(b)}{dy}\right|_{AB} \simeq \frac{3\sigma_{in}}{2\pi(r_0')^2} \frac{AB}{A^{2/3}+B^{2/3}} \frac{1}{1+a(A^{1/3}+B^{1/3})} e^{-b^2/2\beta^2} \left.\frac{dN}{dy}\right|_{PP}. \tag{15}$$

For two equal nuclei, the estimate is then

$$\left.\frac{dN}{dy}\right|_{AB} \simeq 0.64 A^{4/3} \frac{1}{1+2aA^{1/3}} e^{-b^2/2\beta^2} \left.\frac{dN}{dy}\right|_{PP}. \tag{16}$$

The expression (16) will be used in the latter to calculate the rapidity distribution in the light of the SCM.

3. Model-Based Analyses and the Results

The data are obtained from the measurements reported for different collisions at varying energies by the separate groups as stated earlier. With variations in the groups the chosen observables selected were and are different. So, we will have to present our model-based analyses and the results arrived at on its basis in the following subsections.

3.1. *Rapidity distribution in central Pb + Pb collisions at 158A GeV/c*

We calculate the rapidity distribution for the antiprotons in the lead–lead collisions at 158A GeV/c in the light of the SCM and the equation reduces to

$$\left.\frac{dN}{dy}\right|^{\bar{p}}_{\mathrm{Pb+Pb}} = 4.4495 \exp(-0.3044 \sinh y_{\mathrm{cm}}). \tag{17}$$

The solid curve in Fig. 1 depicts the plot of this equation against the experimental data offered by NA49 group (Ref. 10) in the Pb + Pb collisions.

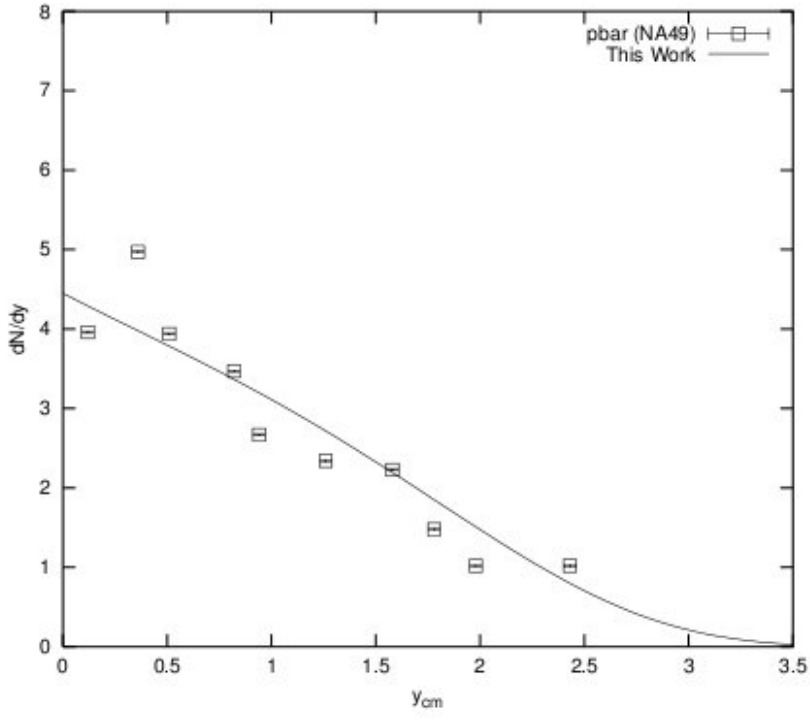

Fig. 1. Plot of rapidity density versus c.m. rapidity for antiprotons (squares) in central Pb + Pb collision at 158A GeV/c reported by NA49 group (Ref. 10). The curve shows the SCM-based theoretical results.

3.2. *Multiplicity ratios of $\bar{p}/\pi$ in central Pb + Pb collisions at 158A GeV/c*

To calculate $\bar{p}/\pi$ ratio in terms of number of participant nucleons ($N_{\rm part}$) in light of SCM, we recall a relation that we had used in our previous work.[19] In that work, $W_A^N(B)$ denotes the number of wounded nucleons in the target nucleus of mass number B, in a collision with a projectile nucleus of mass number A. It has a simple relationship with s, the square of the c.m. energy. The relation is

$$s \cong k[W_A^N(B)]^\alpha \,. \tag{18}$$

Here, k is a product of two terms of which one depends on the nature of the specific secondary particle(s) produced and the other on $1/(AB)^{0.27}$. α, a parameter, depends on the system used. For Pb + Pb collisions $\alpha \simeq 1/0.5103$. In formulating the above relationship (Eq. (18)) we follow the procedural steps used in one of our previous work[19(a)] which was partly based on the work of Kadija *et al.*[19(b)] The cardinal points that are to be reckoned with for calculating the number of wounded nucleons are: (i) one of the prime guiding factors in the nucleus–nucleus collisions is the impact parameter denoted by b, which has a certain limiting relationship with the total cross-section of basic nucleon–nucleon interaction ($\sim \sigma_{NN}/\pi$); (ii) they

arise out of the multiple and consecutive collisions when the nucleons become extremely excited (wounded). Still, they are supposed to behave almost the same as the original nucleons and thus to retain the same cross-section as the original nucleons. So, the number of wounded nucleons would have certain dependence on the basic nucleon–nucleon (NN) total cross-sections through the implicit role of the impact parameters. These two points of physical insights play a significant part in the following calculations; they occur in some or all of the used expressions and also in the deduced results presented hereafter.

In experiments, the factor $W_A^N(B)$ has a correspondence and relationship with the number of participant nucleons ($N_{\rm part}$) representing nucleons that have suffered an "interaction."

Using the value of s given in Eq. (18) and inserting it in Eqs. (2) and (5) we obtain for pions and antiprotons

$$\langle n_{\pi^+}\rangle = \langle n_{\pi^-}\rangle = \langle n_{\pi^0}\rangle \cong 0.1794[W_A^N(B)]^{0.3919}\,, \tag{19}$$

the value of k in Eq. (18) is 0.1630 for pions.

$$\langle n_p\rangle = \langle n_{\bar{p}}\rangle \cong 0.0024[W_A^N(B)]^{0.4899} \tag{20}$$

the value of k in Eq. (18) is 0.12 for antiprotons. The $\bar{p}/\pi$ ratio for different number of participating nucleons are plotted in Fig. 2. The data are taken from Refs. 10 and 20.

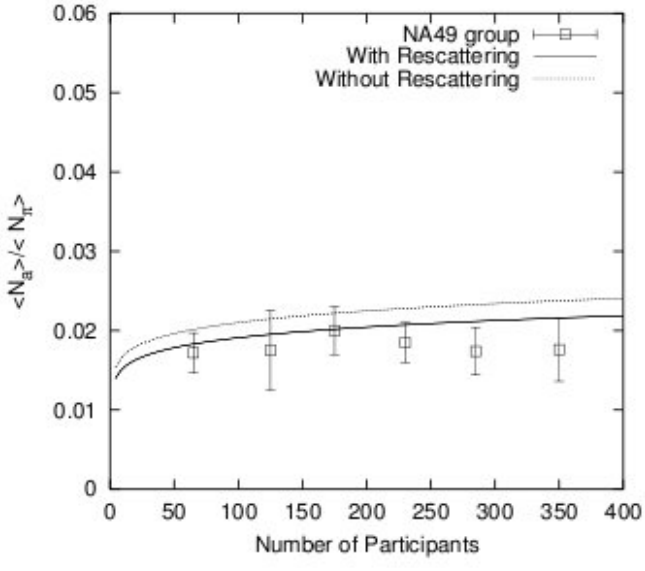

Fig. 2. The preliminary NA49 data on the antiproton to pion ratio in centrally selected Pb + Pb (squares) at 158A Gev/c as a function of number of participants. Data are obtained from Ref. 10. The flat curvilinear line shows the theoretical SCM-based results with rescattering effects whereas the dashed line represents the results without rescattering.

Now, we would consider and introduce empirically the effect of cascading and rescattering of the secondaries produced in ultra-relativistic heavy-ion collisions. There is a certain degree of cascading and rescattering processes[21] which cannot be probably ignored altogether. We assume a fully statistical and charge-independent behavior for cascading and rescattering effects as a first approximation. As we have assumed the collisions to be nearly central, the role of cascading and rescattering should be reckoned with in the overlap regions of the colliding nuclei which might contribute independently to particle production. The role of these two effects is here computed empirically with the reckoning of the factor $\sim (\overline{\nu_k}(A))^{\epsilon}$, with $\epsilon \ll 1$. Here, $\overline{\nu_k}(A)$ is the number of secondary collisions caused by the produced nucleons/particles themselves.

In Fig. 2, we have plotted two lines, one dashed and another solid, with the help of the SCM-based calculated results. The dashed line shows the results without the rescattering effects and the solid line indicates values with an addition of the contribution from the rescattering term.

The model-based plot supports the moderate observance of antiproton scaling ($\bar{p}/\pi$ ratio behavior), though there is and may be a very slow rise of the $\bar{p}/\pi$ ratio with the increasing number of participating nucleons in the nuclei. As there is a stringent upper limit on the participating nucleons depending upon the value(s) of the mass number(s) of the projectile and the target, there is likely to be a saturation of the values of the observable(s) measured in the experiments even at the asymptotic energies.

3.3. *Rapidity distribution of antiprotons in Au + Au collisions at 11.7A GeV/c*

In this subsection we calculate the rapidity distribution of $\bar{p}$ in terms of the number of participating nucleons called wounded nucleons for Au + Au collisions at 11.7A GeV/c. The value of α in Eq. (18) is taken to be $\sim 1/1.64$. Hereafter, combining the equations (4), (7)–(9), (16) and (18) we arrive at the final expression given below

$$\left.\frac{dN}{dy}\right|^{\bar{p}}_{\mathrm{Au+Au}} = 0.165[W_A^N(B)]^{0.013} \exp(-6.74[W_A^N(B)]^{-0.159}). \tag{21}$$

Figure 3 illustrates the results obtained by the above expression. The data points here are taken from Ref. 1. The solid line in that figure shows the theoretical plot by the SCM-based calculated results in the rapidity range $1.0 < y < 2.2$. In data-plotting a beam energy correction factor of 0.47 as a multiplier is applied to cases of both Si + Au and Si + Al collisions. But, we have neglected here the effect of rescattering, as the contribution of this term is found to be very small.

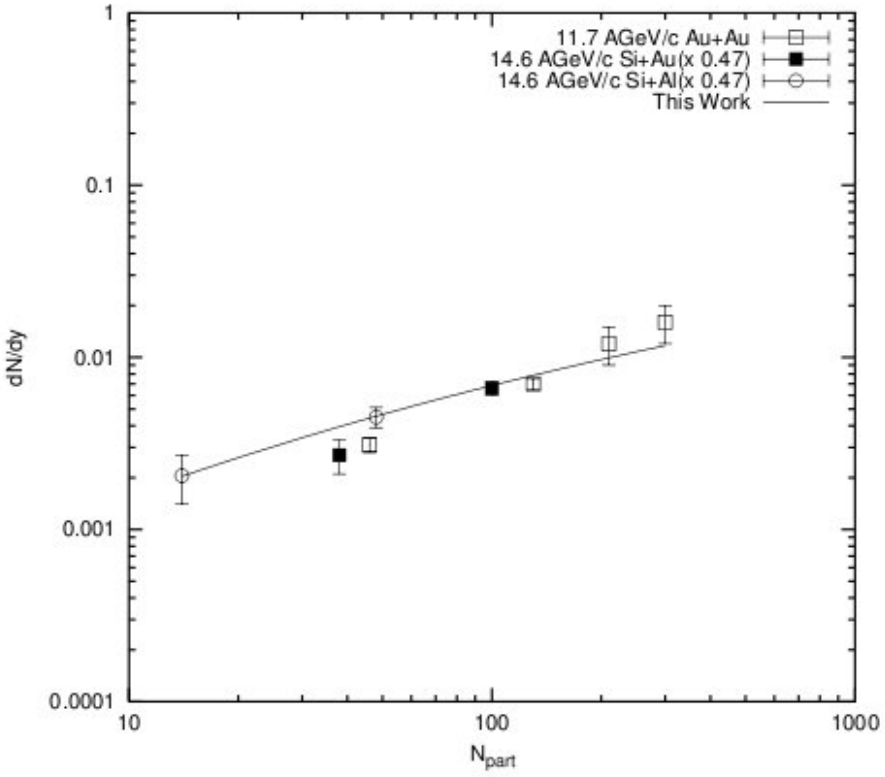

Fig. 3. Plot of data for dN/dy of $\bar{p}$ in Si + A and Au + Au collisions as a function of N_{part}. The data-set is taken from Ref. 1. The line depicts the SCM-based calculated results.

3.4. *Midrapidity antiproton-to-proton ratio from Au + Au collisions at* $\sqrt{s_{NN}} = 130$ *GeV*

In a previous work SB[13] had shown that in a reaction of the type $p+p \to c+x$, the expression for excess production of the protons over antiprotons would be obtained by field theoretic derivations in the form given by

$$(B_p)_{PP} = \frac{4\pi g^2_{NN\pi}}{[(P'+K)^2 - m^2_{p]}{}^2} A(\nu, q^2)_{p_s} \int \frac{d^3k_p}{2(2\pi)^3} \exp(-ik_p x)\,, \tag{22}$$

where the symbols have their contextual connotation with the following hints to the physical reality of an extraneous proton production as one nonleading secondary: the first part consists of a $NN\pi$ coupling strength parameter in the numerator and the denominator is just a propagator term for an excited nucleon. The second term represents the common multiparticle production amplitude along with the extraneous production mode and the last term indicates simply the phase space integration term on the probability of generation of a single proton (as a fermion). This represents the excess production of secondary proton in a specific mode of production shown in Ref. 13.

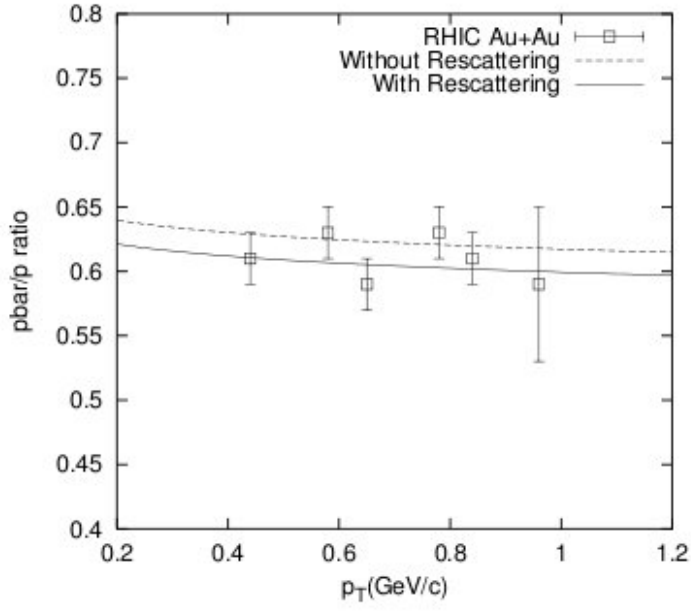

Fig. 4. Representation of the antiproton-to-proton ratio as a function of transverse momentum over the rapidity range $0.3 < |y| < 0.4$ in Au + Au collisions at RHIC. The data points are from Ref. 11. The results arrived at on the basis of SCM are shown by the plot of the solid curve with the inclusion of rescattering effects and the dashed curve represents the results without rescattering.

Now making use of some high-energy approximations we get two relations: one for $\bar{p}/p$ in terms of p_T, another for $\bar{p}/p$ in terms of y in Au + Au collisions at the RHIC at $\sqrt{s_{NN}} = 130$ GeV. The relations are

$$\frac{\bar{p}}{p} = \frac{1}{1 + 0.62(p_T)^{0.06}}\,, \tag{23}$$

and

$$\frac{\bar{p}}{p} = \frac{0.65}{1 + 0.2\sinh y_{\rm cm}}\,. \tag{24}$$

The experimental data are taken from Refs. 9, 11 and 12 and are plotted in Figs. 4 and 5 respectively. The effects of rescattering are considered here purely phenomenologically. The dashed lines in Figs. 4 and 5 represent calculations without rescattering effects whereas the solid line in those figures show the SCM-based calculated results with the inclusion of the rescattering terms. The rapidity variable range in Fig. 4 is taken to be $0.3 < |y| < 0.4$ and the range for p_T is $0.6 < p_T < 0.8$ in Fig. 5. Moreover, in Fig. 6 we plot theoretical $\bar{p}/p$ ratios (both with and without rescattering) for higher values of y against experimental data. The data are taken from the measurements reported by the BRAHMS Collaboration.[22] The data trend observed by the BRAHMS collaboration on the measured antiproton to proton ratio is reflected by our theoretical calculations. A point must be made here that, the

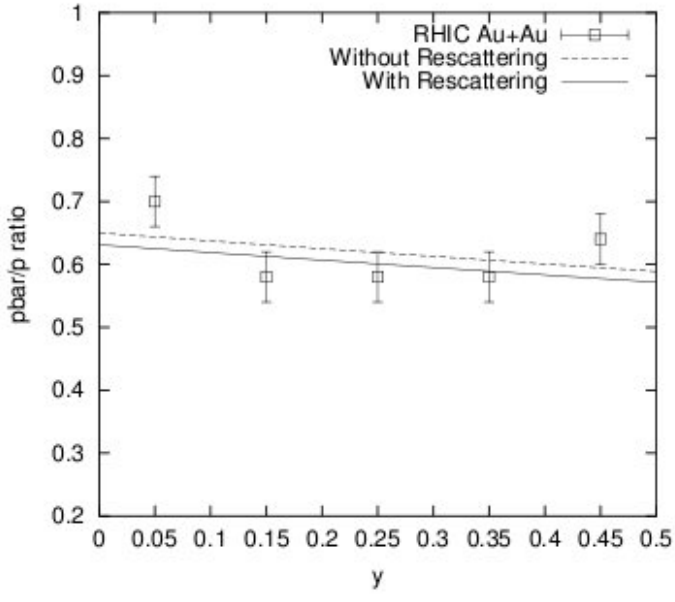

Fig. 5. Depiction of the antiproton-to-proton ratio for Au + Au collisions at RHIC as a function of rapidity within $0.6 < p_T < 0.8$ GeV/c. The data points are from Ref. 11. The theoretical results on the basis of SCM with and without rescattering are drawn as solid and dashed lines respectively.

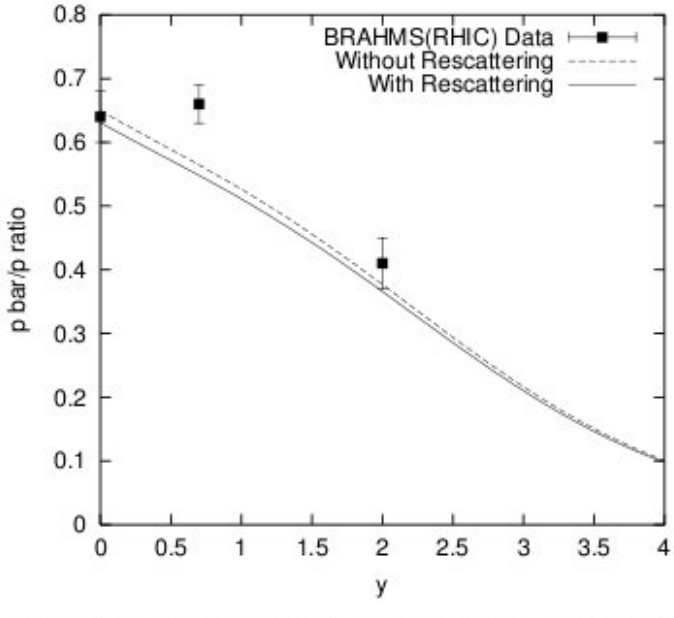

Fig. 6. Comparison of the measured $N(\bar{p})/N(p)$ ratios to model predictions. The data points are from Ref. 22. The theoretical results on the basis of SCM with and without rescattering are drawn as solid and dashed lines respectively.

effect of rescattering does not come out very prominently in the case of $\bar{p}$ measurements reported here. This may be due to sparse data, narrow y-range in the measurements and/or relatively heavy baryonic mass of the detected secondaries.

Now, to understand why $\bar{p}/p$ is always less than unity, we might argue in a way as given hereafter.

With increase of energy of the projectile, the impact of collision on the target nucleus breaks it down to splinters of extremely excited nucleons, that is, energized protons and neutrons. At high energies they do come out along with the produced real secondaries of protons and antiprotons. The detectors, under special circumstances of energy of protons and antiprotons, fail to differentiate between the secondaries — real or virtual, and give measures for mixed variety of protons with pure secondary antiprotons. For antiprotons no additional source through this break-up mechanism does exist. So the ratio would always come to values less than unity with a very slow fall-off.

4. Discussion and Conclusions

Let us now concentrate first to the results on lead-lead collisions at high energies. The fair agreement of the theoretical plot in Fig. 1 on the rapidity density versus c.m. rapidity variable demonstrates the modest validity of the underlying models of (a) nucleon–nucleon collisions and (b) that for transition from NN to AA collisions. In our opinion, the results shown in Fig. 2 are much more revealing from the physical point of view. The solid curve in the diagram of Fig. 2 depicts a very slow rise of the ratio of antiproton-to-pion yield in the Pb + Pb collisions. This means a moderate observance of the antiproton scaling idea. But, one must admit that the rate of rise is far less than what is conjectured by the QGP diagnostic approach. Hereafter, we take up for discussion the results of Au + Au collisions at relatively low energies (compared to that of Pb + Pb collision). The model-based calculations shown by the solid line in Fig. 3 agree nicely with the measurements on Si + Al, Si + Au, and finally, on Au + Au collisions as well. The antiproton yields in the measured energy range of Au + Au collision do not exhibit either experimentally or theoretically any excess production. Finally, we discuss the results from RHIC at higher energies. The plots are in good agreement with measured data depicted in all the three figures (Figs. 4–6). They nicely represent the mean values of the measured physical observables at relatively much higher energy, $\sqrt{s} = 130$ GeV. Quite noticeably, on the effect of cascading and rescattering in the nuclear collisions, the situation appears to be a bit unclear: the $\bar{p}/p$ vs. p_T plot in Fig. 4 exhibits better fits with inclusion of rescattering contributions; whereas, such a case is not clearly made for plots on $\bar{p}/p$ versus y values in Fig. 5 and specially in Fig. 6 for reasons indicated before in the text. So, for arriving at a decisive conclusion, one has to await for further data on the related observables over either wider y or larger p_T values.

The overall impact of all this and their bearing on the evolution of physics of QGP-hypothesis could be summarised by the following statements:

(i) The totality of data do not give any strong hint to the onset of any QGP phase or scenario.
(ii) No clear indication for excess antiproton production is available.
(iii) In high energy nuclear collisions, the role of physics of cascading and rescattering assumes an ambiguous status as hinted before. This is a crucial departure from the typical conventional stand on the issue in question.
(iv) The present work does not pertain to any of the thermodynamic considerations or of the thermal model physics for which we have no comments as such on energy density, entropy or baryochemical potential, chemical freeze-out temperature etc.[23–25] which are some model-specific proposed parameters.
(v) However, the models applied here are capable of explaining satisfactorily the measured and reported data on antiproton production in some high energy nuclear collisions with an altogether different approach which we have dwelled upon in the present work.

Acknowledgments

The authors are very grateful to the anonymous referee for some valued comments and helpful suggestions. One of the authors, P. Guptaroy, is thankful to the UGC (India) for its financial support through the Faculty Development Programme.

References

1. E802 Collaboration (Y. Akiba *et al.*), *Nucl. Phys.* **A610**, 139c (1996); W. Casing, *Acta. Phys. Pol.* **B29**, 3175 (1998); L. Ahle *et al.*, *Phys. Rev. Lett.* **81**, 2650 (1998).
2. S. A. Bass, M. Gyulassi, H. Stocker and W. Greiner, *J. Phys.* **G25**, R1 (1999).
3. H. Sorge *et al.*, *Phys. Lett.* **B243**, 7 (1990).
4. U. Heinz, M. Jacob, nucl-th/0002042.
   Also at: http://cern.ch/CERN/Announcements/2000/NewStateMatter/.
5. M. Bleicher *et al.*, *Phys. Lett.* **B485**, 133 (2000).
6. F. Karsch, E. Laermann and A. Peikert, *Phys. Lett.* **B478**, 447 (2000).
7. X. N. Wang and M. Gyulassy, *Phys. Rev. Lett.* **68**, 1480 (1992).
8. NA44 Collaboration (I. G. Bearden *et al.*), *Phys. Rev. Lett.* **78**, 2080 (1997).
9. STAR Collaboration (K. H. Ackermann *et al.*), *Phys. Rev. Lett.* **86**, 402 (2001).
10. NA49 Collaboration (F. Sikler *et al.*), *Nucl. Phys.* **A661**, 45c (1999); G. Veres *et al.*, *ibid.* **A661**, 383c (1999).
11. C. Adler *et al.*, *Phys. Rev. Lett.* **86**, 4778 (2001).
12. PHENIX Collaboration (K. Adcox *et al.*), *Phys. Rev. Lett.* **86**, 3500 (2001).
13. S. Bhattacharyya, *J. Phys.* **G14**, 9 (1988) and references therein.
14. S. Bhattacharyya, *Il Nuovo Cimento* **C11**, 51 (1988) and references therein.
15. P. Bandyopadhyay and S. Bhattacharyya, *Il Nuovo Cimento* **A43**, 305 (1978) and references therein.
16. A. B. Kaidalov and K. A. Ter Martirosyan, *Sov. J. Nucl. Phys.* **36**, 979 (1984).
17. Particle Data Group, *Eur. Phys. J.* **C15**, 211 (2000).
18. C. Y. Wong, *Introduction to High-Energy Heavy Ion Collisions* (World Scientific, 1994).

19. (a) P. Guptaroy, S. Bhattacharyya, B. De and D. P. Bhattacharyya, *Fizika* **B10**, 103 (2001); (b) K. Kadija, I. Derado, N. Schmitz and P. Seyboth, *Z. Phys.* **C66**, 373 (1995).
20. M. I. Gorenstein, M. Gazdzicki and W. Greiner, *Phys. Lett.* **B483**, 60 (2000).
21. J. Geiss, W. Cassing and C. Greiner, *Nucl. Phys.* **A644**, 107 (1998).
22. BRAHMS Collaboration (I. G. Bearden *et al.*), *Phys. Rev. Lett.* **87**, 112305 (2001).
23. PHOBOS Collaboration (B. B. Back *et al.*), *Phys. Rev. Lett.* **87**, 102301 (2001).
24. PHOBOS Collaboration (B. B. Back *et al.*), *Phys. Rev. Lett.* **87**, 102303 (2001).
25. STAR Collaboration (C. Adler *et al.*), *Phys. Rev. Lett.* **87**, 112303 (2001).